AGU PUBLICATIONS

Geophysical Research Letters

RESEARCH LETTER
10.1002/2015GL067265

Key Points:
- Evidence of an anthropogenic contribution to the drying trend in central Chile
- Anthropogenic forcing explains about a quarter of the 2010–2014 drought in central Chile
- Major PDO effect on the recent large-scale circulation and South Pacific precipitation trends

Supporting Information:
- Text S1, Table S1, and Figures S1–S4

Correspondence to:
J. P. Boisier,
jboisier@dgf.uchile.cl

Citation:
Boisier, J. P., R. Rondanelli, R. D. Garreaud, and F. Muñoz (2016), Anthropogenic and natural contributions to the Southeast Pacific precipitation decline and recent megadrought in central Chile, *Geophys. Res. Lett.*, *43*, 413–421, doi:10.1002/2015GL067265.

Received 2 DEC 2015
Accepted 16 DEC 2015
Accepted article online 17 DEC 2015
Published online 14 JAN 2016

Anthropogenic and natural contributions to the Southeast Pacific precipitation decline and recent megadrought in central Chile

Juan P. Boisier[1,2], Roberto Rondanelli[1,2], René D. Garreaud[1,2], and Francisca Muñoz[2]

[1]Department of Geophysics, Universidad de Chile, Santiago, Chile, [2]Center for Climate and Resilience Research, Universidad de Chile, Santiago, Chile

Abstract Within large uncertainties in the precipitation response to greenhouse gas forcing, the Southeast Pacific drying stands out as a robust signature within climate models. A precipitation decline, of consistent direction but of larger amplitude than obtained in simulations with historical climate forcing, has been observed in central Chile since the late 1970s. To attribute the causes of this trend, we analyze local rain gauge data and contrast them to a large ensemble of both fully coupled and sea surface temperature-forced simulations. We show that in concomitance with large-scale circulation changes, the Pacific Decadal Oscillation explains about half of the precipitation trend observed in central Chile. The remaining fraction is unlikely to be driven exclusively by natural phenomena but rather consistent with the simulated regional effect of anthropogenic climate change. We particularly estimate that a quarter of the rainfall deficit affecting this region since 2010 is of anthropogenic origin. An increased persistence and recurrence of droughts in central Chile emerges then as a realistic scenario under the current socioeconomic pathway.

1. Introduction

The amplitude—and in some cases the direction—of the precipitation response to anthropogenic climate forcing (ACF) remains uncertain in many regions [e.g., *Burke and Brown*, 2008; *Deser et al.*, 2012; *Knutti and Sedlácek*, 2013; *Orlowsky and Seneviratne*, 2013; *Shepherd*, 2014]. In this context, the Southeast Pacific drying represents a particularly robust regional effect of ACF within global climate model (GCM) simulations [*Allen and Ingram*, 2002; *Collins et al.*, 2013]. The physical mechanism behind the modeled precipitation decrease in this region has not been explored in depth but echoes changes in large-scale circulation, notably the Hadley cell widening and the associated poleward displacement of the subtropical dry regimes [*Johanson and Fu*, 2009; *Cai et al.*, 2012; *Grise and Polvani*, 2014].

Given the lack of reliable long-term rainfall information over the oceans, the historical effects of ACF in the Southeast Pacific cannot be properly evaluated with observations. However, the simulated drying in this region also comprises continental areas of southern South America and may therefore be contrasted to land-based data. Indeed, a persistent rainfall deficit has prevailed in central Chile since 2010 to date, leading to a marked decline in water reservoirs and an extended forest fire season, among other effects [*Center for Climate and Resilience Research*, 2015]. This so-called megadrought has no precedents in local records and contributes to a long-standing dry trend in the region (Figure 1) [see also *Minetti et al.*, 2003; *Quintana and Aceituno*, 2006; *Carrasco et al.*, 2008]. Nonetheless, the congruence with model simulations, the nature of the rainfall trend and current drought in Chile, is unclear, since no formal studies of climate change attribution have been carried out specifically in this part of the globe.

To detect and attribute changes in regional precipitation is a challenging task because of the large influence of weather regimes on local rainfall variability and the resulting low signal-to-noise ratio in climate series [e.g., *Burke and Brown*, 2008; *Hoerling et al.*, 2010; *Bindoff et al.*, 2013; *Orlowsky and Seneviratne*, 2013]. Across the Pacific basin and in Chile, particularly, the El Niño–Southern Oscillation (ENSO) and the Pacific Decadal Oscillation (PDO) are key driving factors for precipitation variability at interannual and longer time scales [*Aceituno*, 1988; *Rutllant and Fuenzalida*, 1991; *Garreaud and Battisti*, 1999; *Montecinos and Aceituno*, 2003; *Quintana and Aceituno*, 2012].

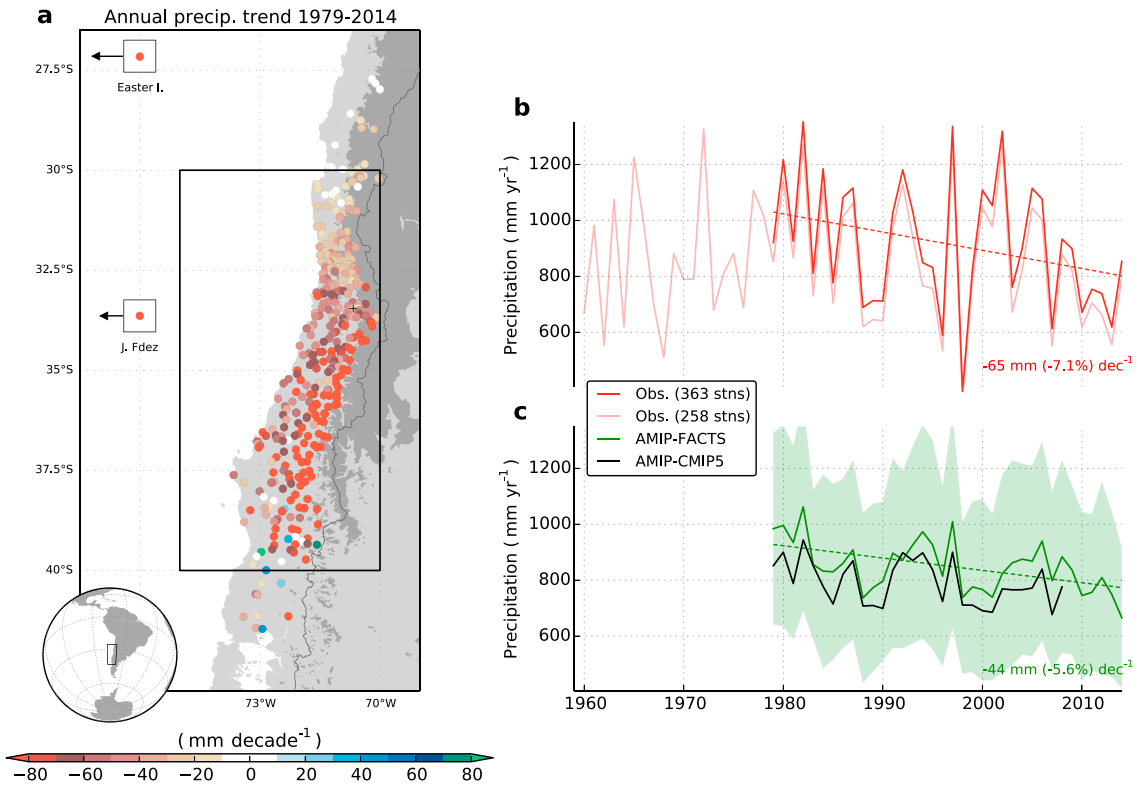

Figure 1. (a) Trends of annual precipitation observed in rain gauge stations in Chile between 1979 and 2014. Time series of annual mean precipitation in central Chile based on (b) rain gauge observations and (c) SST-forced GCM simulations. Dashed lines indicate the corresponding linear precipitation trend from 1979 to 2014. Box in Figure 1a shows domain used for regional average.

The influence of the ACF and sea surface temperature (SST)-driven natural variability on the large-scale circulation and the associated contribution to the drying trend in the Southeast Pacific is the focus of the present study. We specifically quantify the relative role that the PDO and the ACF have played on the precipitation trend in this region since the late 1970s, by analyzing an updated data set of local rain gauge observations in central Chile and a large ensemble of GCM simulations.

2. Data and Methods

We use four types of data in this study: rain gauge observations, gridded observation-based products, reanalyses, and GCM outputs. The rain gauge data gather updated records in Chile from two national agencies: the directorate of water resources (*Dirección General de Aguas*, DGA) and the weather service (*Dirección Meteorológica de Chile*, DMC). Monthly precipitation totals between 1979 and 2014 from 406 stations are retained and analyzed after a quality control and gap-filling procedures (supporting information). A smaller group of 267 stations is also used for long-term precipitation assessments.

Stations between 30°S and 40°S (~90% of the total) are used to compute average precipitation trends in central Chile (Figure 1). To reduce biases induced by the irregular distribution of stations, rainfall averages are first computed on four subregions (the whole region assessed was divided latitudinally) and then combined. Random resampling of the annual mean precipitation time series in central Chile was performed to evaluate the statistical significance of the trends in this region (section 4).

Historical changes in large-scale circulation are evaluated with gridded sea level pressure (SLP) data. The data sets analyzed include the Hadley Centre Sea Level Pressure reconstruction (HadSLP2) [*Allan and Ansell*, 2006] and four reanalysis: the National Centers for Environmental Prediction-Department of Energy (NCEP-DOE) Reanalysis II [*Kanamitsu et al.*, 2002], the NOAA-Cooperative Institute for Research in Environmental Sciences (CIRES) Twentieth Century Reanalysis [*Compo et al.*, 2011], the European Centre for Medium-Range Weather Forecasts (ECMWF) ERA-Interim Reanalysis [*Dee et al.*, 2011], and the ECMWF ERA-20C Reanalysis [*Poli et al.*, 2013].

The model data analyzed include both fully coupled and SST-forced simulations from 26 GCMs participating in Coupled Model Intercomparison Project Phase 5 (CMIP5; see Table S1 in the supporting information). The fully coupled ensemble combines all-forcing historical runs from 1979 to 2005, and Representative Concentration Pathway (RCP) 8.5 scenario runs for the 2006–2014 period [*Taylor et al.*, 2011]. These two simulations are analyzed together as a single run per GCM (hereafter referred to as HIST-CMIP5). Since the internal variability is effectively removed by averaging, the ensemble mean of these simulations is used to evaluate the historical SLP and precipitation responses to external forcing, particularly to ACF.

The SST-forced simulations assessed include the Atmospheric Model Intercomparison Project (AMIP) runs performed for the period 1979–2008 in the context of CMIP5 [*Taylor et al.*, 2011] (hereafter AMIP-CMIP5), as well as an ensemble of AMIP simulations, updated to 2014, done with five models as part of the NOAA Facility for Climate Assessments (AMIP-FACTS, Table S1). The AMIP-CMIP5 runs were carried out with the atmospheric component of each of the 26 GCMs included in HIST-CMIP5 and, except for the observed boundary condition prescribed at the ocean surface, used the same climate forcing — anthropogenic and natural — than the fully coupled runs until 2005. The AMIP-FACTS simulations used are of the same nature as AMIP-CMIP5 (i.e., including both the historical climate forcing and SST) and, despite the fewer GCMs available, include a large number of realizations (120 runs in total, Table S1).

As in the fully coupled simulations, the AMIP-type runs include a variety of different physical parameterizations of the land-atmosphere system and therefore can be used to evaluate the robust effects of ACF. In addition to ACF, the AMIP ensembles are exploited here to evaluate the atmospheric response to observed changes in SST and in underlying phenomena, particularly the PDO.

The PDO is defined as the leading mode of variability of the North Pacific SST [*Mantua et al.*, 1997]. Similarly to other indexes [e.g., *Garreaud and Battisti*, 1999], the PDO is an indicator of ENSO-like decadal-scale climate modulations. In this study, we use a simple linear regression framework to estimate SLP and precipitation changes congruent with the PDO. This estimate is computed for the observations and AMIP simulations, based on the annual time series of the PDO (Figure 2c; we use the index of *Mantua et al.* [1997], available online at http://www.atmos.washington.edu/~mantua/abst.PDO.html). Hence, for a generic variable X in a given location or grid point, the PDO-driven trend is estimated as $\alpha \times \delta$PDO, where δPDO is the linear trend of the PDO index and α is the regression slope computed between the annual time series of the PDO and X.

Following the data availability, the trend analysis considers the periods 1979–2008 (all data) and 1979–2014 (all data but AMIP-CMIP5). The 1979–2008 period is used to compare the fully coupled and SST-forced simulations from the group of CMIP5 GCMs (section 3). The 1979–2014 period is of particular interest since it includes the recent years of persistent rainfall deficit in central Chile (2010–2014; section 4). The PDO-driven trends for this longer period is also extrapolated from the AMIP-CMIP5 runs by using the corresponding (1979–2014) observed PDO trend and the parameter α obtained with the regression analysis of the period 1979–2008. To allow the comparison at regional scale, all models and observation-based fields were first interpolated to a common rectangular grid of 1.0° latitude-longitude.

3. Changes in Large-Scale Circulation and Southeast Pacific Drying

Climate variability in Chile is primarily controlled by the circulation and weather regimes prevailing over the South Pacific. Hence, to evaluate the precipitation changes in this region, we first look at the historical evolution of the large-scale circulation and calculate the linear trend in annual SLP between 1979 and 2008.

The observed and simulated global distribution of SLP trends, as well as the estimated PDO contribution to these trends, are shown in Figure 2. A robust pattern of SLP changes is evident in the observational data sets evaluated here, in spite of important differences among them (Figure S1) [see also *Gillett et al.*, 2013]. This pattern has positive (negative) trends in the eastern (western) tropical and subtropical Pacific, as well as a clear weakening of the Aleutian Low (Figure 2a). Furthermore, the observed SLP trends are fairly consistent with those simulated in AMIP-CMIP5 (Figure 2d) and with expected — La Niña-like — response to changes in PDO between 1979 and 2008 (Figures 2b and 2e). Indeed, after an abrupt shift in the 1970s from a negative to a positive phase, the PDO has gradually evolved toward a negative phase during the last three decades (Figure 2c).

The north-south contrasting SLP trend in the Southeast Pacific is a PDO fingerprint of particular interest in this study since it enlightens the mechanism behind rainfall deficits in central Chile expected for a negative PDO

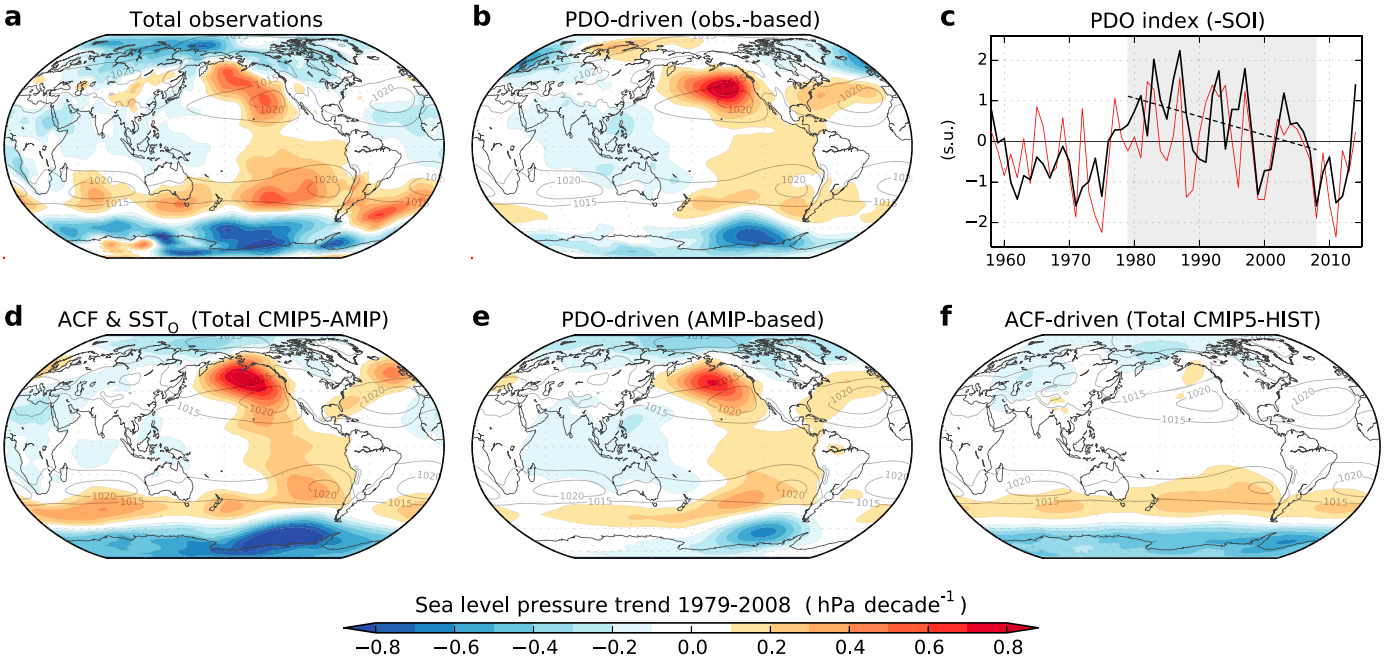

Figure 2. Ensemble mean trends (1979–2008) of annual sea level pressure (SLP) from five observational products and 26 CMIP5 GCM simulations. Total trends (a) observed and (d) simulated in AMIP-CMIP5. PDO-driven trends derived from (b) the observations and (e) the AMIP-CMIP5 ensemble. (f) Total trends simulated in HIST-CMIP5. Contour lines indicate the corresponding climatological mean SLP (in hPa). (c) Standardized annual indices of the PDO (black) and SOI (sign inverted; red). Dashed line indicates the linear trend of the PDO between 1979 and 2008.

phase (Figures 2b and 2e). The opposite pattern, a blocking high over the Bellingshausen Sea and a weakened South Pacific anticyclone, is a well-known atmospheric condition favoring an anomalously northward position of the storm track and rainfall superavit in central Chile during *El Niño* years [*Karoly*, 1989; *Rutllant and Fuenzalida*, 1991; *Sinclair et al.*, 1997; *Renwick*, 1998; *Montecinos and Aceituno*, 2003].

The correspondence between the PDO-driven and the total SLP trends both in the observations and in AMIP simulations reveals the PDO as a key driver of large-scale circulation trends at the time scale considered. In addition to the PDO signal, the observed SLP trends and simulated in AMIP-CMIP5 exhibit a circumpolar pattern of change in the southern mid- and high latitudes (Figures 2a and 2d) in agreement with the trends shown by the HIST-CMIP5 ensemble (Figure 2f). This zonally symmetric component—a positive Southern Annular Mode-like pattern of change—is a well-known response of austral circulation to ACF reported in several observational studies [e.g., *Thompson et al.*, 2000; *Marshall*, 2003; *Arblaster and Meehl*, 2006; *Gillett et al.*, 2013; *Lee and Feldstein*, 2013] and shown in model projections [e.g., *Fyfe et al.*, 1999; *Arblaster et al.*, 2011; *Gillett and Fyfe*, 2013].

To quantify the ACF and PDO contribution to the large-scale precipitation changes in the South Pacific/South America sector, we follow the same procedure used for SLP (Figure 3). Here, however, we have refrained from evaluating precipitation trends based on reanalysis or satellite-derived products given their major biases [*Yin et al.*, 2004; *Trenberth et al.*, 2011].

The annual precipitation trends simulated from 1979 to 2008 in AMIP-CMIP5 indicate a clear drying belt spanning from the central tropical Pacific to southwestern South America (Figure 3a). In this case, a remarkable similar spatial configuration, but of lower amplitude, is found both in the PDO-congruent component of this trend (Figure 3c) and in the simulated effect of ACF (HIST-CMIP5) during the same period (Figure 3d). The question that arises here is whether the precipitation responses to ACF and to changes in the PDO are linear and how these two drivers contribute to the total trends simulated and observed from 1979 to 2008. The sum of the two components shows indeed a great correspondence with the total trends simulated in AMIP-CMIP5 (cf. Figures 3a and 3b). This result is somehow surprising considering that the simple attribution approach followed here is not based on an ad hoc modeling experiment but on independent simulations of different nature (fully coupled and SST forced).

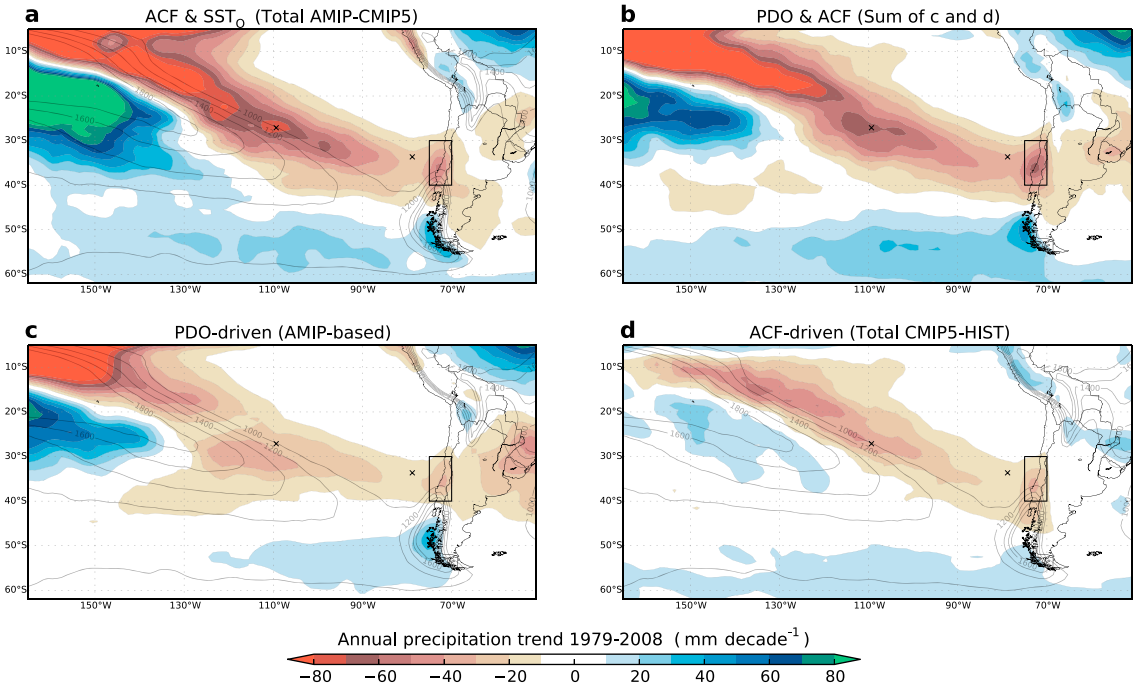

Figure 3. Ensemble mean trends (1979–2008) of annual precipitation derived from 26 CMIP5 GCM simulations in the Southeast Pacific. (a) Total and (c) PDO-driven trends derived from AMIP-CMIP5 simulations. (d) Total trends simulated in HIST-CMIP5. (b) Sum of the PDO and ACF components shown in Figures 3c and 3d. Contour lines indicate the corresponding climatological mean precipitation (in mm yr^{-1}). Cross marks indicate the position of Juan Fernández archipelago and Easter Island.

4. Precipitation Decline in Central Chile: Significance and Attribution

The AMIP-CMIP5 ensemble indicates a dipole of positive/negative precipitation trends in southern/central Chile (Figure 3a). Given the scarcity of observations south of 40°S, we did not assess precipitation changes in austral Chile. We note, however, that there is some evidence of moderate wet trends and glacier thickening in western Patagonia (~50°S) consistent with model simulations [*Möller et al.*, 2007; *Garreaud et al.*, 2013].

Within a large interannual variability, the observed precipitation in central Chile indicates a similar behavior than the PDO: a positive trend between the 1960s and 1980s and a negative trend during the last three decades (Figure 1). We note that the river streamflow data in this region show mostly decreasing trends, in line with the dominating rainfall decline (see supporting information Figure S2). Since 1979, the observed drying is roughly consistent with the trends simulated in AMIP (see Figures 1 and 3a). The negative precipitation trends observed in Robinson Crusoe (Juan Fernández archipelago) and Easter islands are in agreement with the model results too (Figure 1a).

In spite of the widespread signal, the precipitation trends observed in central Chile since 1979 show some dispersion (Figure 1a); a number of stations indicate strong annual rainfall decreases (below −80 mm decade^{-1}), notably across the Andes foothill, while others show weak and even positive trends in the southern limits of the region assessed (Figure 1a). To carry out a quantitative comparison with the GCM simulations, we defined a region within 30–40°S and 70–75°W (see box in Figures 1a and 3) to average the modeled and the observed data (section 2). This comparison is done for the linear precipitation trend in two periods: 1979–2008 (Figure 4a) and 1979–2014 (Figure 4b), as well as for the mean precipitation anomaly during the recent years of persistent deficit (2010–2014, Figure 4c). To dampen differences induced by climatological biases, the observed and simulated precipitation trends and anomalies are in this case expressed in relative terms (i.e., with respect to the corresponding long-term means).

The observations in central Chile indicate a regional mean precipitation trend of −3.7% decade^{-1} between 1979 and 2008 (dashed line in Figure 4a). Given the large rainfall variability in this region (Figure 1b), this trend falls within a probable range and does not require a special explanation besides chance (first column in Figure 1a). Apart from the statistical significance, is it possible to conclude something robust about the

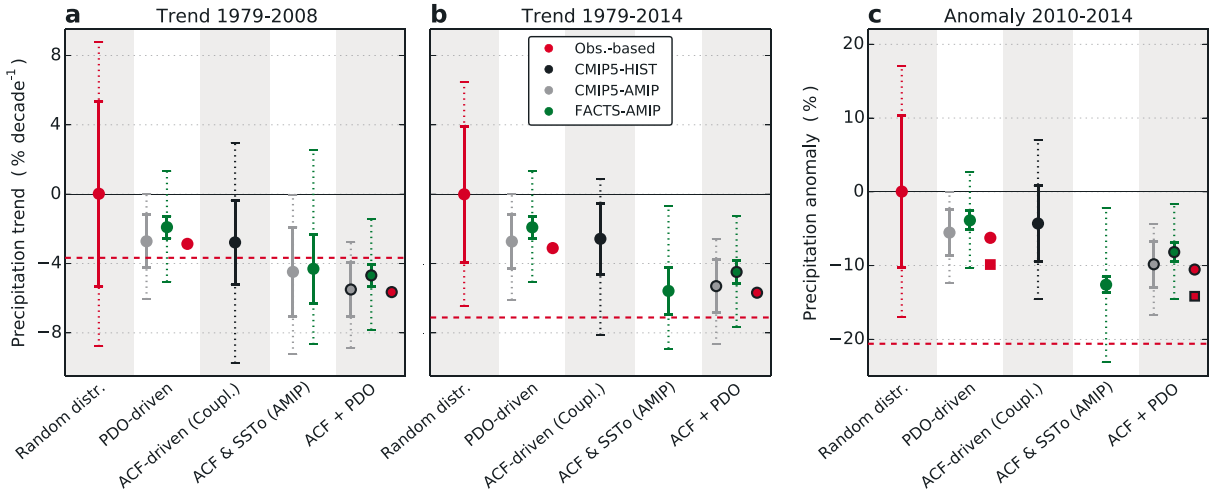

Figure 4. Annual mean precipitation trends in central Chile for the periods (a) 1979–2008 and (b) 1979–2014. Dashed lines in red indicate the mean trend computed from local rain gauge stations. Dots and error bars indicate the mean (μ) ±1.0 standard deviation (σ) trends derived from synthetic time series (observation-based Monte Carlo experiments, in red) and from GCM simulations (legend and *x* axis labels indicate the corresponding ensemble; details in text). Solid error bars indicate the model statistics ($\mu \pm \sigma$) based on the ensemble means of each GCM. Dotted error bars indicate the 5th to 95th percentile range derived from single runs. Dots in red indicate the PDO-driven trends computed with the observations. (c) As in Figures 4a and 4b but for the annual mean precipitation anomaly between 2010 and 2014. In addition to the estimated PDO component based on observations (red dot), the red square shows the estimated anomaly induced by the Southern Oscillation. Right-hand columns in each panel display the observed/simulated PDO component plus the simulated (model-mean) ACF effect in the corresponding metric.

driving mechanisms of this trend? On the one hand, the estimated contribution of the PDO computed with the observations indicates a rainfall decline of 2.8% decade^{-1} (red dot in the second column in Figure 4a), very close to the corresponding AMIP-based estimates (gray and green plots). On the other hand, the simulated ACF-induced trend (total HIST-CMIP5, third column in Figure 4a) shows a drying of 2.8 ± 2.4% decade^{-1}. The total trends simulated in AMIP-CMIP5 and AMIP-FACTS are in good agreement (fourth column in Figure 4a). The drying trend shown by both ensembles and the arithmetic sum of the PDO and ACF trend components (fifth column in Figure 4a) are of slightly larger amplitude than observed but in agreement considering the intermodel spread.

As shown in Figures 3 and 4a, the amplitude of the 1979–2008 precipitation trend shown by the AMIP ensembles in the Southeast Pacific and in central Chile appears to be partially explained by the PDO and ACF, with a roughly 50/50 contribution. However, the driving factors explaining the ensemble mean trends are not necessarily valid for a single model run or the observations, where natural phenomena other than the PDO may also contribute. This issue and the different model rainfall sensitivities to the PDO (see supporting information Figure S3) explain part of the large dispersion within the ensemble members. As a consequence, the observed 1979–2008 trend cannot be clearly attributed and could indeed be easily explained both by the PDO and by the ACF individually (Figure 4a).

A different diagnosis is drawn when the trend analysis is updated to 2014. The amplitude of the rainfall decline observed in central Chile between 1979 and 2014 (7.1% decade^{-1}; Figure 4b) is almost twice the 1978–2008 one and statistically significant (p<0.05). Additionally, the trend for this longer period is unlikely driven by the PDO nor by the ACF alone; the two drivers foresee a similar decline equivalent to about 40% of the observed one (second and third columns in Figure 4b). In turn, the total trend shown by the AMIP-FACTS ensemble (−5.6 ± 1.4%), although of weaker magnitude than the observations, is fairly consistent considering the ensemble spread.

In summary, the observed drying trend in central Chile reconciles with model results only if the anthropogenic forcing and the observed SST changes are accounted for jointly. The 1979–2014 trends resulting from the sum of the PDO and ACF components (fifth column in Figure 4b) agree with those simulated in FACTS-AMIP, confirming the PDO as the leading SST-mediated cause of slow (multidecadal) rainfall variations in this region. We note that 14% of the AMIP-FACTS runs show a drying of larger amplitude than observed, suggesting the atmospheric internal variability as an additional natural driver of the actual rainfall trend.

5. Discussion and Conclusions

The large amplitude of the 1979–2014 precipitation trend in central Chile is to some extent weighted by the recent years of persistent rainfall deficit (Figure 1b). To inquire into the role of ACF and natural variability on this megadrought, the same framework and linear regression model used for the trend analysis (Methods) are applied to assess the 5 year rainfall anomaly between 2010 and 2014 (Figure 4c). The result resembles the one obtained for the 1979–2014 trend. In this case, a Monte Carlo test of significance places the 2010–2014 deficit (−21%) as an extremely rare event ($p < 0.01$). The PDO-driven estimate of this anomaly, as well as the expected (modeled) ACF contribution, account for only a quarter of the observed anomaly. Hence, the simple linear reasoning indicates that the PDO and the ACF explain altogether about half of the actual drought (see fifth column in Figure 4c).

Unlike multidecadal trends, phenomena of shorter time scale than the PDO have a greater influence on 5 year anomalies. We looked particularly at the ENSO contribution to the 2010–2014 deficit, using the Southern Oscillation index (SOI) instead of the PDO in our analysis (SOI is one of the ENSO metrics that explain the larger rainfall anomaly in central Chile, Figure S3). Indeed, compared to the PDO, the SOI-driven precipitation anomaly (about −10%; see red square in Figure 4c) explains a larger fraction of the total anomaly. Even so, the observed ENSO contribution combined with the modeled ACF effect indicates an anomaly of weaker amplitude than observed (fifth column in Figure 4c). We note that the PDO accounts for most of the long-term ENSO variability and trends (Figure 2c), so the contributions of the two phenomena are not additive.

The estimated ACF+SOI contribution to the 2010–2014 anomaly agrees well with what is simulated in AMIP-FACTS ($-12.6 \pm 1.1\%$, 4th column in Figure 4c). Hence, besides the ENSO-like perturbations, the evolution of SST worldwide does not seem to contribute significantly to this anomaly. It is clear from Figure 4c that in addition to ACF, SST variability and associated phenomena, internal atmospheric variability plays an important role in explaining the amplitude of the current drought. Indeed, ∼25% of AMIP-FACT simulations show rainfall deficits above 15%, and 11% of the runs show even larger anomalies than observed. This particular group of simulations is not explored further here but should provide clarity in the final causes of the current rainfall deficit. Yet the main point of this study is that anthropogenic forcing, even not being the leading driver, is critical to explain the drying trend in central Chile and, likely, a key factor behind the persistence of the current drought. The evidence of an emerging anthropogenic effect on the precipitation regime in central Chile is therefore a bold conclusion, with major implications for the country's water resources.

Given the model uncertainties (Figure S3) and the large rainfall variability in central Chile (Figure 1), it is difficult to shed light on the real local rainfall sensitivity to greenhouse gas forcing and other ACF. State-of-the-art GCMs forced with the high-emission scenario RCP8.5 project to 2050 a precipitation deficit of 15–20% in central Chile [*Collins et al.*, 2013]. Hence, following the present-day global activities and related fossil fuel emissions, the current megadrought may anticipate the midterm future conditions in this region.

The method applied to evaluate historical precipitation changes across the Southeast Pacific makes a valuable use of a multimodel data set, notably the AMIP simulations. Similar analyses may also serve to understand climate trends in other regions having high dependance to large-scale SST conditions. Given the climate similarities and the influence of the PDO, we repeated our analyses to look at the causes of precipitation trends in western North America (see supporting information Figure S4). The transient change toward a negative PDO phase explains remarkably well the drying trends simulated in the North Pacific from 1979 to 2008. The modeled trend agrees with the observations in western U.S. (notably in California), and in contrast to what both the GCMs and observations show in central Chile, there is no robust ACF signal there. This complementary result then reaffirms the conclusions from several other studies showing natural variability as the leading factor for the recent rainfall deficits in western North America [e.g., *Wang and Schubert*, 2014; *Delworth et al.*, 2015; *Seager et al.*, 2015].

Acknowledgments
This study received financial support from CONICYT (Chile) through the FONDECYT grants 3150492 (J.P.B.) and 1140637 (R.G.), and through the FONDAP Research Center (CR)2 (15110009). An updated rain gauge and river streamflow data set were provided by the Chilean agencies DGA and DMC. We acknowledge the World Climate Research Programme's Working Group on Coupled Modelling, which is responsible for CMIP, and we thank the climate modeling groups (listed in Table S1) for producing and making available their model output. For CMIP the U.S. Department of Energy's Program for Climate Model Diagnosis and Intercomparison provides coordinating support and led development of software infrastructure in partnership with the Global Organization for Earth System Science Portals. The ensemble of AMIP-FACTS simulations is available at http://www.esrl.noaa.gov/psd/repository/alias/facts/. Suggestions from an anonymous reviewer helped to improve an earlier version of this study.

References

Aceituno, P. (1988), On the functioning of the Southern Oscillation in the South American Sector. Part I: Surface climate, *Mon. Weather Rev.*, *116*(3), 505–524, doi:10.1175/1520-0493(1988)116<0505:OTFOTS>2.0.CO;2.

Allan, R., and T. Ansell (2006), A new globally complete monthly Historical Gridded Mean Sea Level Pressure Dataset (HadSLP2): 1850–2004, *J. Clim.*, *19*(22), 5816–5842, doi:10.1175/JCLI3937.1.

Allen, M. R., and W. J. Ingram (2002), Constraints on future changes in climate and the hydrologic cycle, *Nature*, *419*(6903), 224–232, doi:10.1038/nature01092.

Arblaster, J. M., and G. A. Meehl (2006), Contributions of external forcings to southern annular mode trends, *J. Clim.*, *19*(12), 2896–2905, doi:10.1175/JCLI3774.1.
Arblaster, J. M., G. A. Meehl, and D. J. Karoly (2011), Future climate change in the Southern Hemisphere: Competing effects of ozone and greenhouse gases, *Geophys. Res. Lett.*, *38*, L02701, doi:10.1029/2010GL045384.
Bindoff, N. L., et al. (2013), Detection and attribution of climate change: From global to regional, in *Climate Change 2013: The Physical Science Basis. Contribution of Working Group I to the Fifth Assessment Report of the Intergovernmental Panel on Climate Change*, edited by T. F. Stocker et al., pp. 867–952, Cambridge Univ. Press, Cambridge, U. K., and New York, doi:10.1017/CBO9781107415324.022.
Burke, E. J., and S. J. Brown (2008), Evaluating uncertainties in the projection of future drought, *J. Hydrometeorol.*, *9*(2), 292–299, doi:10.1175/2007JHM929.1.
Cai, W., T. Cowan, and M. Thatcher (2012), Rainfall reductions over Southern Hemisphere semi-arid regions: The role of subtropical dry zone expansion, *Sci. Rep.*, *2*, 702, doi:10.1038/srep00702.
Carrasco, J. F., R. Osorio, and G. Casassa (2008), Secular trend of the equilibrium-line altitude on the western side of the southern Andes, derived from radiosonde and surface observations, *J. Glaciol.*, *54*(186), 538–550, doi:10.3189/002214308785837002.
Center for Climate and Resilience Research (2015), Mega-drought (2010–2015): A lesson to the future. report for policymakers (in Spanish) prepared by the Center for Climate and Resilience Research (CR)2, Chile. [Available online at www.cr2.cl/megasequia.]
Collins, M., et al. (2013), Long-term climate change: Projections, commitments and irreversibility, in *Climate Change 2013: The Physical Science Basis. Contribution of Working Group I to the Fifth Assessment Report of the Intergovernmental Panel on Climate Change*, edited by T. F. Stocker et al., pp. 1029–1136, Cambridge Univ. Press, Cambridge, U. K., and New York.
Compo, G. P., et al. (2011), The twentieth century reanalysis project, *Q. J. R. Meteorol. Soc.*, *137*(654), 1–28, doi:10.1002/qj.776.
Dee, D. P., et al. (2011), The ERA-Interim reanalysis: Configuration and performance of the data assimilation system, *Q. J. R. Meteorol. Soc.*, *137*(656), 553–597, doi:10.1002/qj.828.
Delworth, T. L., F. Zeng, A. Rosati, G. A. Vecchi, and A. T. Wittenberg (2015), A link between the hiatus in global warming and North American drought, *J. Clim.*, *28*(9), 3834–3845, doi:10.1175/JCLI-D-14-00616.1.
Deser, C., R. Knutti, S. Solomon, and A. S. Phillips (2012), Communication of the role of natural variability in future North American climate, *Nat. Clim. Change*, *2*(11), 775–779, doi:10.1038/nclimate1562.
Fyfe, J. C., G. J. Boer, and G. M. Flato (1999), The Arctic and Antarctic oscillations and their projected changes under global warming, *Geophys. Res. Lett.*, *26*(11), 1601–1604, doi:10.1029/1999GL900317.
Garreaud, R., and D. S. Battisti (1999), Interannual (ENSO) and interdecadal (ENSO-like) variability in the Southern Hemisphere tropospheric circulation*, *J. Clim.*, *12*(7), 2113–2123, doi:10.1175/1520-0442(1999)012<2113:IEAIEL>2.0.CO;2.
Garreaud, R., P. Lopez, M. Minvielle, and M. Rojas (2013), Large-scale control on the Patagonian climate, *J. Clim.*, *26*(1), 215–230, doi:10.1175/JCLI-D-12-00001.1.
Gillett, N. P., and J. C. Fyfe (2013), Annular mode changes in the CMIP5 simulations, *Geophys. Res. Lett.*, *40*, 1189–1193, doi:10.1002/grl.50249.
Gillett, N. P., J. C. Fyfe, and D. E. Parker (2013), Attribution of observed sea level pressure trends to greenhouse gas, aerosol, and ozone changes, *Geophys. Res. Lett.*, *40*, 2302–2306, doi:10.1002/grl.50500.
Grise, K. M., and L. M. Polvani (2014), Is climate sensitivity related to dynamical sensitivity? A Southern Hemisphere perspective, *Geophys. Res. Lett.*, *41*, 534–540, doi:10.1002/2013GL058466.
Hoerling, M., J. Eischeid, and J. Perlwitz (2010), Regional precipitation trends: Distinguishing natural variability from anthropogenic forcing, *J. Clim.*, *23*(8), 2131–2145, doi:10.1175/2009JCLI3420.1.
Johanson, C. M., and Q. Fu (2009), Hadley cell widening: Model simulations versus observations, *J. Clim.*, *22*(10), 2713–2725, doi:10.1175/2008JCLI2620.1.
Kanamitsu, M., W. Ebisuzaki, J. Woollen, S.-K. Yang, J. J. Hnilo, M. Fiorino, and G. L. Potter (2002), NCEP–DOE AMIP-II Reanalysis (R-2), *Bull. Am. Meteorol. Soc.*, *83*(11), 1631–1643, doi:10.1175/BAMS-83-11-1631.
Karoly, D. J. (1989), Southern Hemisphere circulation features associated with El Niño–Southern Oscillation events, *J. Clim.*, *2*(11), 1239–1252, doi:10.1175/1520-0442(1989)002<1239:SHCFAW>2.0.CO;2.
Knutti, R., and J. Sedlácek (2013), Robustness and uncertainties in the new CMIP5 climate model projections, *Nat. Clim. Change*, *3*(4), 369–373, doi:10.1038/nclimate1716.
Lee, S., and S. B. Feldstein (2013), Detecting ozone- and greenhouse gas-driven wind trends with observational data, *Science*, *339*(6119), 563–567, doi:10.1126/science.1225154.
Mantua, N. J., S. R. Hare, Y. Zhang, J. M. Wallace, and R. C. Francis (1997), A Pacific interdecadal climate oscillation with impacts on salmon production, *Bull. Am. Meteorol. Soc.*, *78*(6), 1069–1079, doi:10.1175/1520-0477(1997)078<1069:APICOW>2.0.CO;2.
Marshall, G. J. (2003), Trends in the Southern Annular Mode from observations and reanalyses, *J. Clim.*, *16*(24), 4134–4143, doi:10.1175/1520-0442(2003)016<4134:TITSAM>2.0.CO;2.
Minetti, J. L., W. M. Vargas, A. G. Poblete, L. R. Acuña, and G. C. Grande (2003), Non-linear trends and low frequency oscillations in annual precipitation over Argentina and Chile, *Atmosfera*, *16*(2), 1931–1999.
Möller, M., C. Schneider, and R. Kilian (2007), Glacier change and climate forcing in recent decades at Gran Campo Nevado, southernmost Patagonia, *Ann. Glaciol.*, *46*(1), 136–144, doi:10.3189/172756407782871530.
Montecinos, A., and P. Aceituno (2003), Seasonality of the ENSO-related rainfall variability in central Chile and associated circulation anomalies, *J. Clim.*, *16*(2), 281–296, doi:10.1175/1520-0442(2003)016<0281:SOTERR>2.0.CO;2.
Orlowsky, B., and S. I. Seneviratne (2013), Elusive drought: Uncertainty in observed trends and short- and long-term CMIP5 projections, *Hydrol. Earth Syst. Sci.*, *17*(5), 1765–1781, doi:10.5194/hess-17-1765-2013.
Poli, P., et al. (2013), The data assimilation system and initial performance evaluation of the ECMWF pilot reanalysis of the 20th-century assimilating surface observations only (ERA-20C), *ERA Rep. Ser. 14*. ECMWF, Shinfield Park, Reading, U. K. [Available at http://www.ecmwf.int/en/research/publications.]
Quintana, J., and P. Aceituno (2006), Trends and interdecadal variability of rainfall in Chile. paper presented at 8th ICSHMO Foz do Iguacu, pp. 371–372, INPE, Brazil, 24–28 Apr.
Quintana, J. M., and P. Aceituno (2012), Changes in the rainfall regime along the extratropical west coast of South America (Chile): 30–43°S, *Atmosfera*, *25*(1), 1–22.
Renwick, J. A. (1998), ENSO-related variability in the frequency of South Pacific blocking, *Mon. Weather Rev.*, *126*(12), 3117–3123, doi:10.1175/1520-0493(1998)126<3117:ERVITF>2.0.CO;2.
Rutllant, J., and H. Fuenzalida (1991), Synoptic aspects of the central Chile rainfall variability associated with the Southern Oscillation, *Int. J. Climatol.*, *11*(1), 63–76, doi:10.1002/joc.3370110105.
Seager, R., M. Hoerling, S. Schubert, H. Wang, B. Lyon, A. Kumar, J. Nakamura, and N. Henderson (2015), Causes of the 2011 to 2014 California drought, *J. Clim.*, *28*, 6997–7024, doi:10.1175/JCLI-D-14-00860.1.

Shepherd, T. G. (2014), Atmospheric circulation as a source of uncertainty in climate change projections, *Nat. Geosci.*, *7*, 703–708, doi:10.1038/ngeo2253.

Sinclair, M. R., J. A. Renwick, and J. W. Kidson (1997), Low-frequency variability of Southern Hemisphere sea level pressure and weather system activity, *Mon. Weather Rev.*, *125*(10), 2531–2543, doi:10.1175/1520-0493(1997)125<2531:LFVOSH>2.0.CO;2.

Taylor, K. E., R. J. Stouffer, and G. A. Meehl (2011), An overview of CMIP5 and the experiment design, *Bull. Am. Meteorol. Soc.*, *93*(4), 485–498, doi:10.1175/BAMS-D-11-00094.1.

Thompson, D. W. J., J. M. Wallace, and G. C. Hegerl (2000), Annular modes in the extratropical circulation. Part II: Trends, *J. Clim.*, *13*(5), 1018–1036, doi:10.1175/1520-0442(2000)013<1018:AMITEC>2.0.CO;2.

Trenberth, K. E., J. T. Fasullo, and J. Mackaro (2011), Atmospheric moisture transports from ocean to land and global energy flows in reanalyses, *J. Clim.*, *24*(18), 4907–4924, doi:10.1175/2011JCLI4171.1.

Yin, X., A. Gruber, and P. Arkin (2004), Comparison of the GPCP and CMAP merged gauge-satellite monthly precipitation products for the period 1979–2001, *J. Hydrometeorol.*, *5*(6), 1207–1222, doi:10.1175/JHM-392.1.

Wang, H., and S. Schubert (2014), Causes of the extreme conditions over California during early 2013 [in "Explaining extremes of 2013 from a climate perspective"], *Bull. Am. Meteorol. Soc.*, *95*(9), S7–S11.